Chapter 28
Experimental and Numerical Investigation of Blade Angle Variation on a Counter-Rotating Tidal Current Turbine

Lee Nak-Joong, Kim In-Chul, Hyun Beom-Soo and Lee Young-Ho

Abstract Importance of renewable energy has become paramount due to its perennial source and no adverse environmental impact. Ocean is one of the major source of renewable energy where the sun's energy is converted into various natural phenomenon. Southwestern sea in particular, in Korea, has large range of tidal currents with potential for tidal current power generation. Tidal power has great potential for future power and electricity generation because of the massive size of the oceans. The major benefit of tidal power and difference from most renewable energy sources is that it is independent of seasons and weather, that is, it is always constant which makes power generation predictable and makes tidal power a reliable energy source. Horizontal-axis-type turbine appears to be the most technologically and economically viable option for the generation of tidal power. Several studies have shown that single-rotor turbines can obtain a theoretical maximum power coefficient of 59.3 %, whereas dual rotor can obtain a maximum of 64%. Hence, with the optimization of counter-rotating turbines, more power can be obtained than the single-rotor turbines.

Previous studies focus on the performance analysis of the turbine with the variation of distance between the blades. This chapter primarily concentrates on the investigation of the performance analysis and power output of a counter-rotating current turbine by the variation of blade angles by both computational fluid dynamics (CFD) simulation and experiments. Numerical simulations were performed using a commercial finite volume method solver, ANSYS CFX ver.13.0. Experiments were conducted in the water tank with a vertically circulating water channel in

L. Young-Ho (✉)
Division of Mechanical and Energy System Engineering,
Korea Maritime and Ocean University, Busan, Korea
e-mail: lyh@kmou.ac.kr

L. Nak-Joong · K. In-Chul
Department of Mechanical Engineering, Graduate School,
Korea Maritime and Ocean University, Busan 606-791, Korea

H. Beom-Soo
Division of Naval Architecture and Ocean System Engineering,
Korea Maritime and Ocean University, Busan, Korea

A. Sayigh (ed.), *Renewable Energy in the Service of Mankind Vol I*,
DOI 10.1007/978-3-319-17777-9_28

the laboratory of Korea Maritime and Ocean University (KMOU) to validate the numerical results. Several experiments were conducted with the fixed front blade angle and varying the rear blade angle and vice versa at various water flow rate. Surface streamlines, torque, total power output, power coefficient (C_p) etc., were characterized and compared for CFD and experimental cases. The results obtained find good agreement with each other.

Keywords Blade angle · Counter rotating · Current turbine · CFD · Experiment

28.1 Introduction

Renewable energy is reliable and plentiful and will potentially be very cheap once technology and infrastructure improve. Many countries are looking to increase the share of renewable energy to their total consumption these days. It includes solar, wind, geothermal, hydropower, and tidal energy plus biofuels that are grown and harvested without fossil fuels. Ocean is one of the major source of renewable energy, where the sun's energy is converted into various natural phenomenon. Southwestern sea in particular, in Korea, has tidal currents with potential for tidal current power generation. Tidal power generation is predictable and tidal power a reliable energy source because it does not rely on weather or seasons. Tidal turbines are placed in areas with high tidal movements, and are designed to capture the kinetic motion of the ebbing and surging of ocean tides to produce electricity. The surrounding marine environment is not disturbed significantly as seawater is still able to flow naturally through the tidal current turbines as it produces power from the water velocity. The horizontal-axis-type turbine appears to be the most viable option at this stage. Single-rotor turbines are calculated to have a theoretical efficiency of 59.3%; a dual rotor turbine can obtain a maximum of 64%. Hence, with the optimization of counter-rotating turbines, more power can be obtained than single-rotor turbines.

According to blade element momentum theory (BEMT), a three-bladed 40-W horizontal-axis-type marine current turbine was designed. This turbine is used for small-scale experimental tests to analyze its performance characteristics. The turbine is planned to be scaled up to a size to produce 10 kW within a submerged floating structure in future.

Previous experiments on tidal turbines had focused on the effect of varying the distance between the front and rear blades on the power characteristics of the turbine. This research work solely focuses on the effects of changing the front and rear blade angles on the performance of the turbine.

Along with the experimental results, the turbine setup and experimental conditions are simulated using a commercial computational fluid dynamics (CFD) software. The results from both CFD calculations and experimental investigations are compared and further discussed in this chapter.

28.2 Numerical Procedure

A 40-W horizontal-axis three-bladed tidal current turbine was designed using BEMT. Figure 28.1 shows the single airfoil of NACA-63-421 with various twist angles and chord length (left) and three-dimensional (3D) modeling of a blade (right). The turbine has the diameter (D) of 500 mm with designed rotational speed of 190 rpm. The rated water speed was 1 m/s.

Figure 28.2 shows the 3D model of the counter-rotating turbines and the experimental setup. Figure 28.3 (left) shows the computational grid of the turbine. The distance from the blade to the inlet, top, and outlet was 3, 5, and 7 times, respectively, the diameter of blade. Single blade was meshed with the remaining blades accounted for by periodic conditions. The nondimensional distance of the first node from the wall or the y-plus value was less than 5 in this calculation with approximately 6.2 million nodes in the hexahedral mesh.

Figure 28.3 (right) shows the computational domain used for the simulation. k–ω shear stress transport (SST) turbulence model was used, and all the calcula-

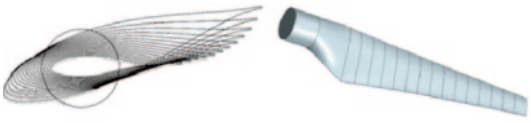

Fig. 28.1 3-D rotor blade configuration

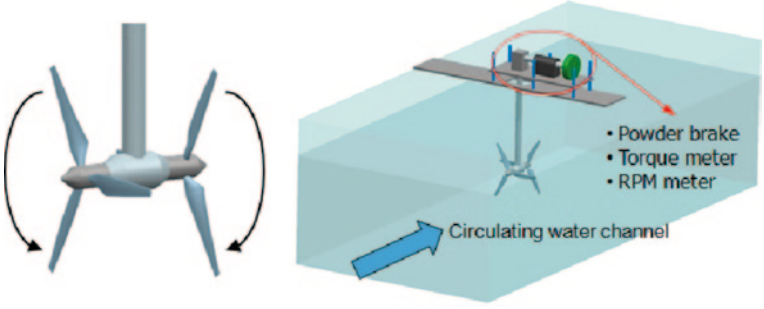

Fig. 28.2 3-D turbine configuration. *RPM* revolutions per minute

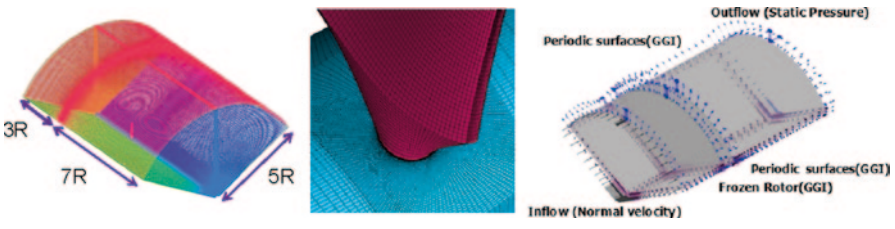

Fig. 28.3 Computational mesh and domain of rotor blade

tions were conducted under steady-state condition using a commercial finite volume method solver, ANSYS CFX ver.13.0. The water velocity was varied from 0.8 to 2.0 m/s during simulation.

28.3 Experimental Procedure

Experiments were conducted in the water tank with a vertically circulating water channel located in the laboratory of KMOU. The height, width, and length of the tank was 1200, 1800, and 4000 mm, respectively. Height of the water level used for this experiment was 900 mm. Figure 28.4 shows the water channel, the turbine, control panel for the channel, and the two fans used to control the water velocity in the water channel. Figure 28.5 shows a schematic diagram of the experimental setup.

Fig. 28.4 Circulating water channel

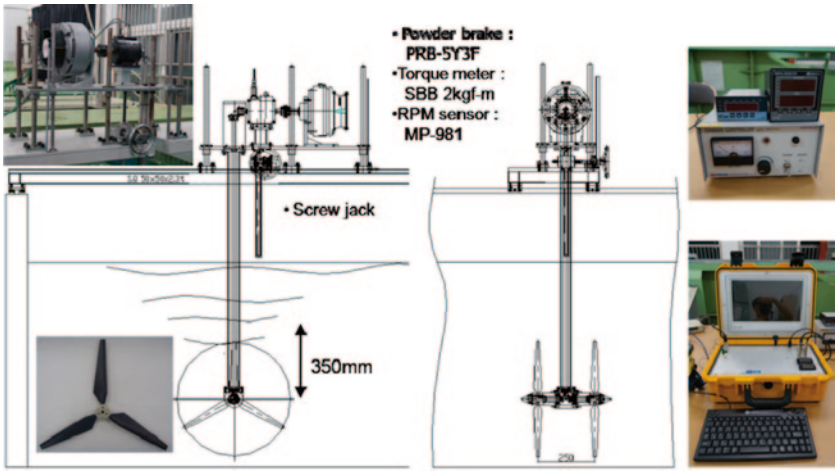

Fig. 28.5 Schematic of the experimental setup

Powder brake, torque transducer, and revolutions per minute (RPM) sensor were attached in the turbine setup for measurement, and the data were recorded in the data logger. The torque meter (model SBB) had a measurement range from 0 to 2 kgf m. The torque meter contained an RPM sensor (MP-981) with a measurement range of up to 10,000 rpm. A forced air-cooled-type powder brake (model PRB-5Y3F) was used to control the RPM of the turbine.

The blockage ratio of the system was 12%. Therefore, a blockage correction factor was applied to the results [4, 6]. Experiments were conducted by varying the water flow from 0.6 to 1.4 m/s. Pitot tube kept at 1 m in front of the turbine was deployed to measure water velocity. The distance between the dual rotors was fixed at 0.5 D.

Aluminum was used as the material for blades, and each blade was fabricated from a single piece using a five-axis milling machine. The total number of blades manufactured was six.

28.4 Results

Figure 28.6 depicts the streamlines observed at the suction side of front and rear blades at a water velocity of 0.8–2.0 m/s in which the arrows indicate the direction of the flow. The arrangement is such that the front blade (F) is positioned at 0° and the rear blade (R) at −5°. Both blades show stable flow over the blade surface with little to no turbulent flow at lower velocities; whereas, as the flow velocity increases, the flow becomes less likely to remain stable on the surface. Flow separation can be seen on the front blade from 1.2 to 2.0 m/s. The nature of streamlines suggest that the flow at rear blade does not separate to the extent as in the front blade. The major reason behind this can be due to the reduction of velocity in the wake of the front blade. Figure 28.7 shows the suction side streamlines for front and rear blades both fixed at 0° to the flow obtained from CFD calculations. In this, the flow remains stable below the design speed of 1 m/s in a similar pattern as described earlier for

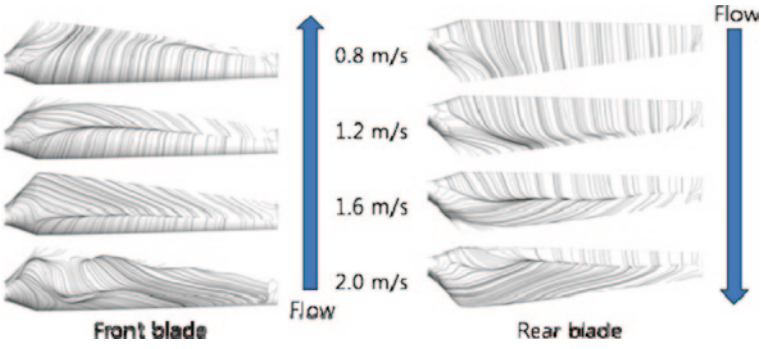

Fig. 28.6 Suction side surface streamlines (F=0°, R=−5°)

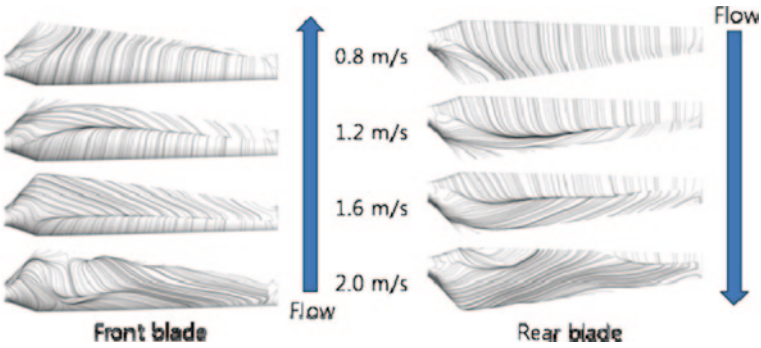

Fig. 28.7 Suction side surface streamlines ($F=0°$, $R=0°$)

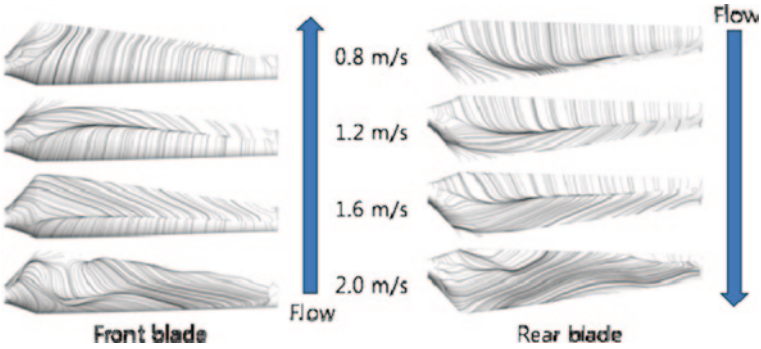

Fig. 28.8 Suction side surface streamlines ($F=0°$, $R=5°$)

Fig. 28.6. As the water velocity increases, the flow also becomes more turbulent over the surface of both blades. The flow was observed to be more turbulent on the rear blade than the previous one at 2.0 m/s. Figure 28.8 shows the streamlines from the CFD calculations when the rear blade was angled at 5° to the flow, while the front blade was fixed at 0°. The flow pattern over the front blade surface shows that it was quite similar to the previous cases (Figs. 28.6 and 28.7), whereas the rear blade shows the increase in turbulent flow occurrence for all water velocities. Figures 28.9 and 28.10 show the surface streamlines cases when the rear blade is fixed at 0°. Figure 28.9 shows the streamlines when the front blade is at −5° to the incoming flow. At water velocity of 0.8 m/s, there is relatively a lesser amount of turbulent flow on both the blades. But as the velocity increases, the flow begins to separate on the front blade much earlier than the rear. The flow on the rear blade does not fully become turbulent until 2 m/s. Figure 28.10 shows the surface flow on the blades when the front blade is angled at 5°. In this case, it can be observed that the flow on the front blade does not completely separate at higher velocities, and the streamlines show that the most of the flow stays on the blade at the lower velocities. But the rear blade streamlines are similar to the previous cases.

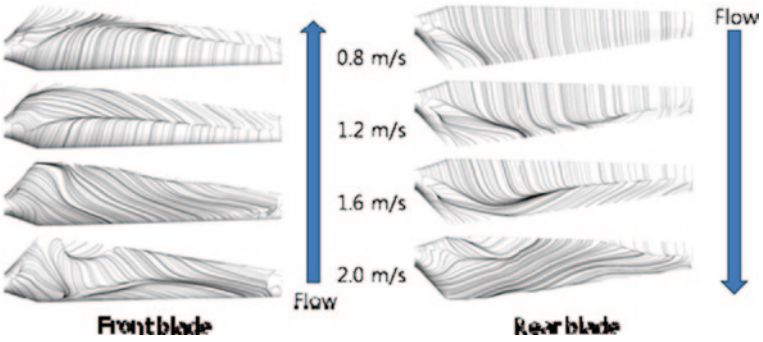

Fig. 28.9 Suction side surface streamlines ($F=-5°$, $R=0°$)

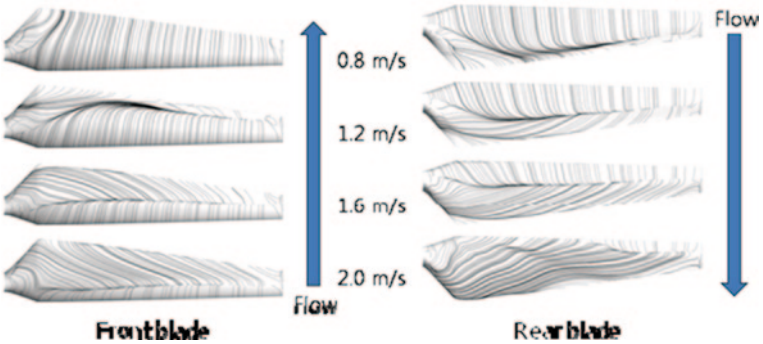

Fig. 28.10 Suction side surface streamlines ($F=5°$, $R=0°$)

Figure 28.11 shows the comparison between the power output developed during the experiments and obtained by CFD calculations at varied water velocities with the fixed front blade at 0° and varying rear blade. The limitation of the experimental setup was that it was unable to produce water velocities larger than 1.4 m/s. However, velocities over this speed caused a lot of problems as sudden stoppage in operation of the water channel during experimentation. The trends of the graph show that both experiment and CFD results are in good agreement over all velocities. The experimental results showed slightly lower power from 0.8 to 1.1 m/s, but slightly higher power at velocities over this range. It was observed that difference between power produced was little when the rear blade angle was changed except at 2.0 m/s. The maximum power obtained from CFD was about 183 W at 1.8 m/s when the rear blade angle was positioned at 5°.

The comparison between the power coefficients (C_p) obtained from CFD calculations and experimental result at a fixed front blade angle is presented in Fig. 28.12. The nature of the graph suggests that the power coefficient obtained from experimental data is lower than the CFD results. The difference between the power coefficients can be easily noticed in the graph as the rear angle is altered. For both

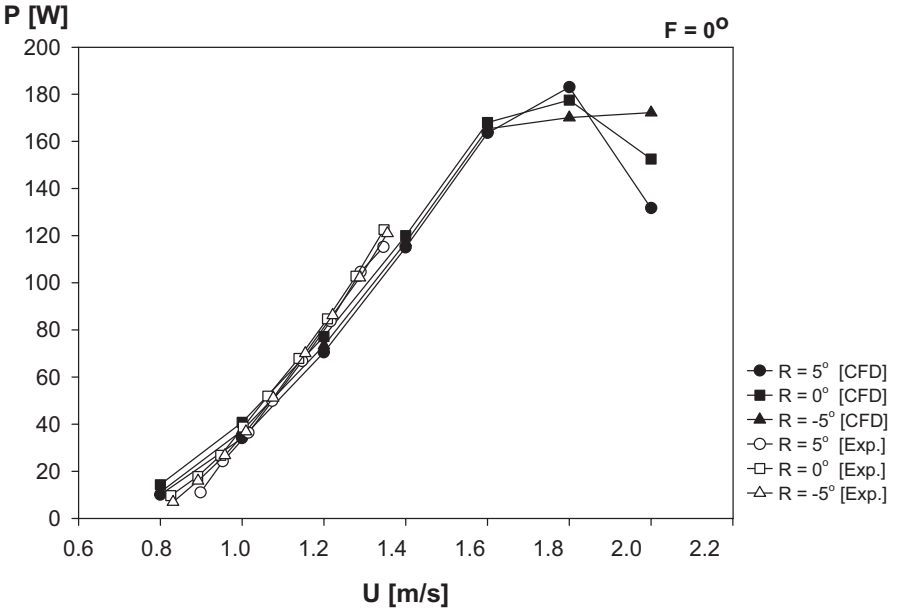

Fig. 28.11 Power output comparison between CFD and experiments (F=0°, R is varied). *CFD* computational fluid dynamics, *Exp* experimental

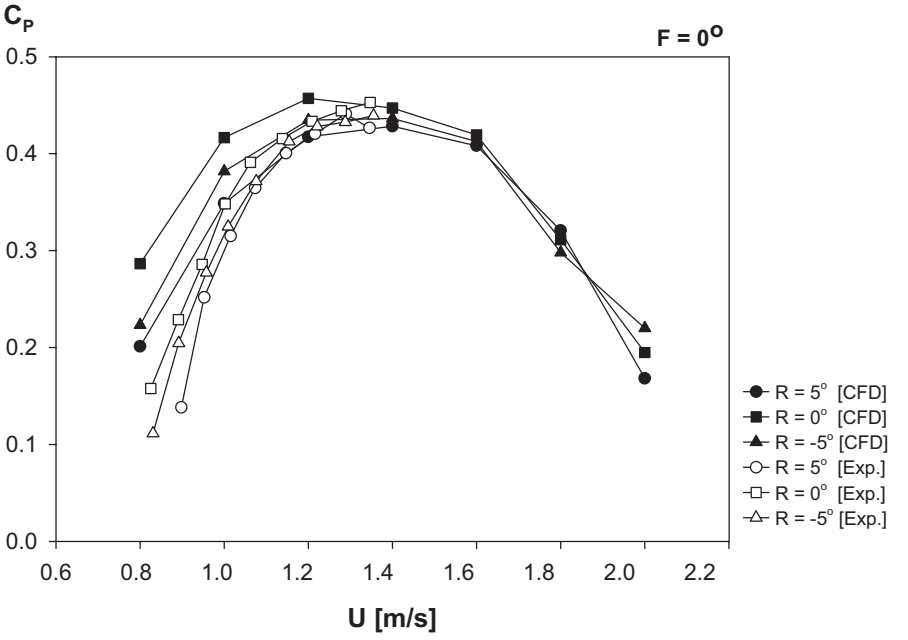

Fig. 28.12 Power coefficient (C_p) comparison between CFD and experiment (F=0°, R is varied). *CFD* computational fluid dynamics, *Exp* experimental

experiments and CFD calculations, high-power coefficients are produced as both the front and rear angles are positioned at 0° to the flow. The trend clearly shows an increase in power coefficient as the water velocities increase until a maximum is reached around 1.2–1.4 m/s and then decreases until 2.0 m/s. The highest power coefficient value of 0.457 was obtained at 1.2 m/s from CFD, whereas it was 0.453 at 1.4 m/s water velocity from experiments.

Figure 28.13 shows the power output comparison of the turbine between CFD and experimental results when the front blade angle is varied, while the rear blade angle is fixed at 0°. Each case shown in this figure shows the increase in power output as the velocity increases until around 1.4 m/s before decreasing until 2 m/s. This drop can be accounted for the loss of flow stability on the front blade shown by the streamlines. The graph shows the close agreement between the CFD and experimental results. As the experiments were conducted up to the water velocity of 1.4 m/s, only CFD data are plotted above this velocity. The power output obtained is 123.514 and 123.405 W from CFD and experiments, respectively, at 1.4 m/s when the front blade is angled at 5°, the value being almost equal. The maximum power attained is 258 W at 2 m/s water velocity for front angle at 5°.

Figure 28.14 shows the plot of power coefficient (C_p) versus the water velocity as the rear blade is fixed. The graph obtained when the front blade is angled at 5° show the higher values of power coefficient compared to other cases. For this case, the maximum C_p obtained from CFD and experiment is 0.460 at 1.4 m/s and 0.461 at 1.302 m/s water velocity, respectively. When both blade angles are fixed at 0°, maximum C_p obtained is 0.457 at 1.2 m/s for the CFD case and 0.461 at 1.302 m/s

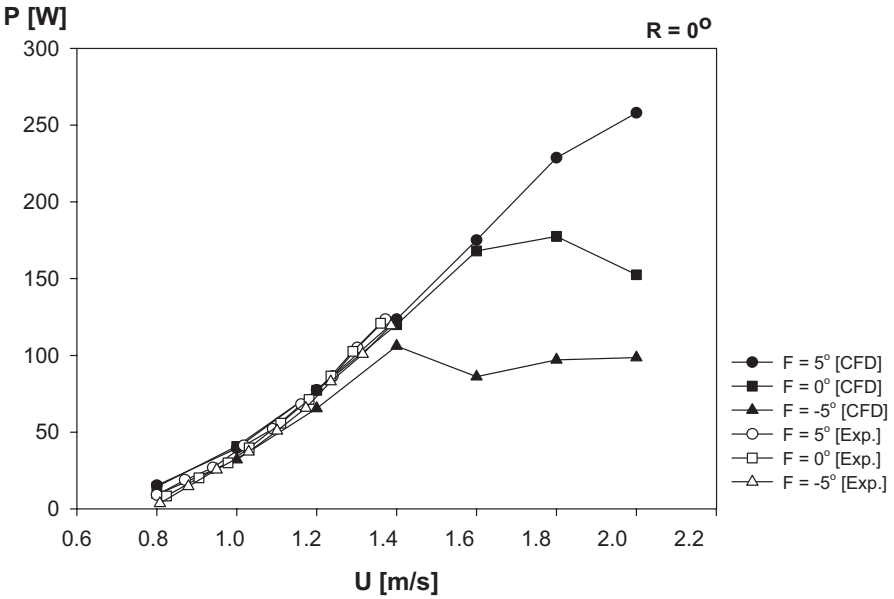

Fig. 28.13 CFD of the power characteristics when the R=0°, front blade (F) angle is varied

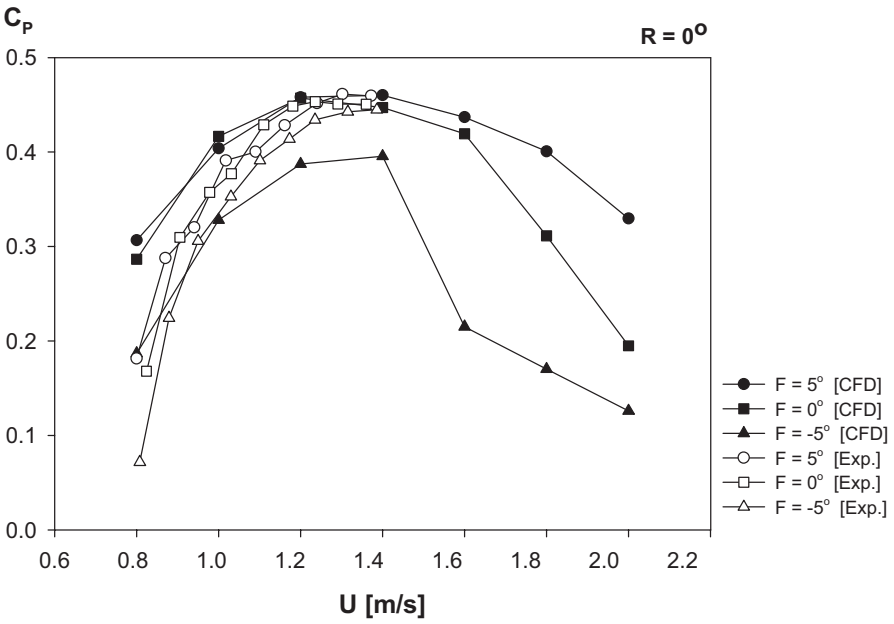

Fig. 28.14 Power coefficient (C_p) comparison between CFD and experiment ($R = 0°$, F is varied). *CFD* computational fluid dynamics, *Exp* experimental

for the experimental case. In contrast, when the blade is angled at −5°, the values of C_p is much lower compared to other two cases in which maximum C_p obtained is 0.395 at 1.4 m/s for the CFD case and 0.445 at 1.372 m/s for experimental case. The highest power output obtained during the experiment was 123.405 W for 1.372 m/s water velocity.

Figures 28.15 and 28.16 show the torque versus the water velocity for both blades for all the CFD cases. Torque produced by the front and rear blades when the front blade angle is fixed at 0° with the rear blade angle varied is presented in Fig. 28.15, whereas Fig. 28.16 depicts the same parameters with rear blade angle fixed at 0° and the front blade angle varying. The data obtained suggest that at lower velocities, there is the occurrence of counter torque. As the velocity increases, the counter torque is removed and the value of torque increases significantly. This phenomenon of counter torque might be related with the starting water velocity and torque balance in the system.

28.5 Conclusions

To determine the effects of blade angle changes on the performance characteristics of the tidal current turbine, CFD analysis was done. Experiments were conducted in the water tank with a vertically circulating water channel at KMOU to validate

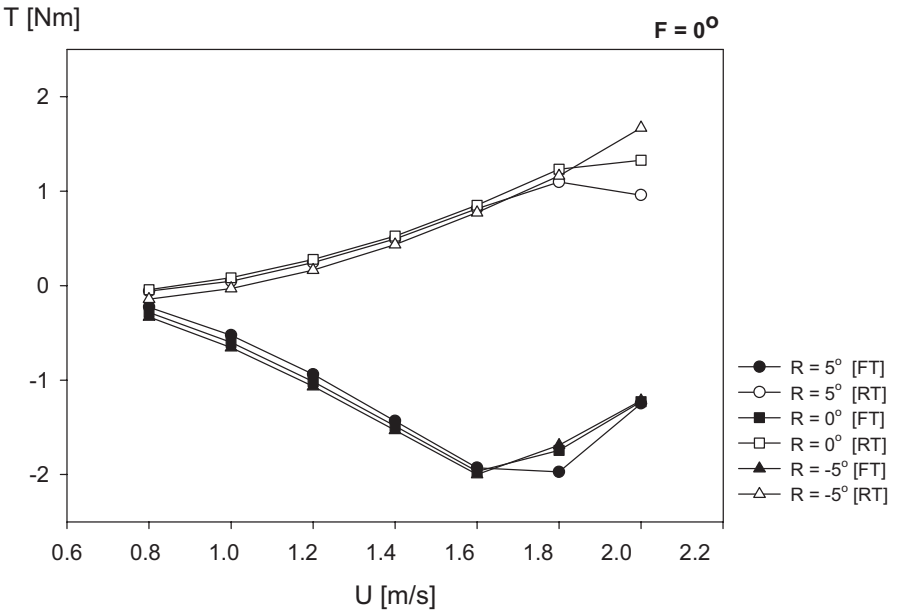

Fig. 28.15 Torque produced by the front blades and rear blades (F=0°, R is varied). *FT* front torque, *RT* rear torque

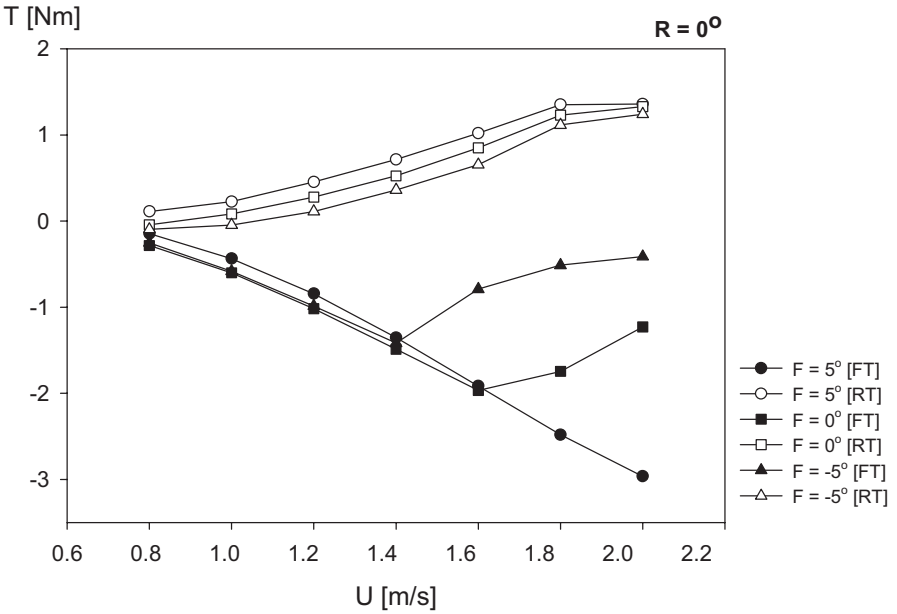

Fig. 28.16 Torque produced by the front blades and rear blades (R=0°, F is varied). *FT* front torque, *RT* rear torque

the numerical results. Streamlines provided the flow pattern over the front and rear blades at various water velocities when the front blade angle was fixed, while the rear blade angle was varied from −5° to 5° and vice versa. The pattern suggests that as the rear blade angle increases, more turbulent the flow becomes. The trends of the graph show that both experiment and CFD results are in good agreement over all velocities. When the front blade was fixed, experimental results showed slightly lower power from 0.8 to 1.1 m/s but slightly higher power at velocities over this range. Also, when the rear blade angle was fixed and the front blade varying, 5° front blade angle showed better flow stability on the surface. The power outputs produced and power coefficients obtained were also presented for the abovementioned cases. Power output from CFD and experiment was 115 W at 1.4 m/s with maximum C_p of 0.46 and 115.17 W with maximum C_p of 0.45, respectively, when the front blade was fixed. Similarly, when the rear blade was fixed, the power output from CFD and experiment was 123.5 W at 1.4 m/s and 123.41 W at 1.37 m/s, respectively, with maximum C_p of 0.46 for both.

Acknowledgments This work was supported by the New and Renewable Energy Core Technology Program of the Korea Institute of Energy Technology Evaluation and Planning (KETEP), granted financial resource from the Ministry of Trade, Industry and Energy, Republic of Korea (20133030000260).

References

1. Ng K-W, Lam W-H, Ng K-C (2013) 2002–2012: 10 years of research progress in horizontal-axis marine current turbines. Energies 6(3):1497–1526
2. Hyun BS, Jo CH, Kim MC, Moon CJ (2011) Technology status and prospect of tidal current power generation. Bull Soc Naval Architects Korea 48(3):12–19
3. Kim BG, Kim CJ, Choi MS (2012) A study on the performance of an 100kW class tidal current turbine. J Korean Soc Marine Environ Safety 18(2):145–152
4. Bahaj AS, Molland AF, Chaplin JR, Batten WMJ (2007) Power and thrust measurements of marine current turbines under various hydro dynamic flow conditions in a cavitation tunnel and a towing tank. J Renew Energy 32(3):407–426
5. Batten WMJ, Bahaj AS, Molland AF, Chaplin JR (2007) Experimentally validated numerical method for the hydrodynamic design of horizontal axis tidal turbines. Ocean Eng 34(7):1013–1020
6. Chen TY, Liou LR (2011) Blockage corrections in wind tunnel tests of small horizontal-axis wind turbines. Exp Therm Fluid Sci 35(3):565–569
7. Coiro DP, Maisto U, Scherillo F, Melone S, Grasso F (2006) Horizontal axis tidal current turbine: numerical and experimental investigations. Proceeding of Offshore wind and other marine renewable energies in Mediterranean and European seas, European Seminar, Rome, Italy
8. Kim BS, Yang CJ, Kim JH, Lee YH (2005) Software development for the optimum rotor design and the performance analysis of the HAWT by BEMT. Trans Korean Soc Mech Eng 5:3141–3146
9. Yang CJ Optimal rotor blade design for tidal in-stream energy. J Korean Soc Mar Environ Safety 17(1):75–82